chemistry proceedings

MDPI

*Proceeding Paper*

# Pharmacophore Modeling of AHAS Inhibitors for Targeted Antifungal Discovery †

**Radu Daniel Savulescu *, Ana Borota * and Sorin Alin Marinescu**

"Coriolan Dragulescu" Institute of Chemistry of the Romanian Academy, 24 M. Viteazu Avenue, 300223 Timisoara, Romania; sorin.alin.marinescu@gmail.com

* Correspondence: rsavulescu@acad-icht.tm.edu.ro (R.D.S.); ana_borota@acad-icht.tm.edu.ro (A.B.)

† Presented at the 30th International Electronic Conference on Synthetic Organic Chemistry, 5–19 November 2026; Available online: https://sciforum.net/event/ecsoc-30/home.

**Abstract**

Recent experimental studies have proven the efficacy of targeting the acetohydroxyacid synthase (AHAS) enzyme against fungal and bacterial infections. Since AHAS is a vital enzyme for plants and microorganisms but absent in animals, it offers a highly selective target with a low risk of human toxicity. Our study aims to deepen the understanding of the molecular mechanisms involved in the inhibition of this enzyme (especially in the *Candida albicans* strain), as well as to extract the essential features responsible for the targeted biological activity. To this end, a suite of pharmacophore models was developed using integrated *in silico* methods. The approach included structure-based molecular docking techniques using the Glide module, and pharmacophore modeling via the Phase module. Structural hypotheses were built based on the specific interactions between a series of known inhibitors and key residues within the enzyme's active site. As a result, an ensemble of 30 distinct pharmacophore hypotheses was generated, each configured to include between 3 and 5 pharmacophore features. The validation of these multiple models (including through atom-based QSAR methods and active-decoy analyses) demonstrated a high capacity to differentiate truly active compounds from inactive molecules. The obtained validated models can be successfully used as efficient filters in virtual screening campaigns for the discovery and optimization of novel compounds with high antifungal potential. This diversified approach maximizes the chances of identifying new efficient chemical structures while simultaneously guaranteeing an optimal safety profile.

**Keywords:** acetohydroxyacid synthase; *Candida albicans*; herbicide; molecular docking; pharmacophore hypothesis; antifungal potential

## 1. Introduction

Acetohydroxyacid synthase (AHAS), also known as acetolactate synthase (ALS), catalyzes the first common step in the biosynthesis of the branched-chain amino acids valine, leucine, and isoleucine. Because this pathway is present in plants, fungi, and bacteria but absent in animals, AHAS represents an attractive target for the development of selective herbicides and antimicrobial agents [1]. Genetic disruption of the AHAS-encoding ILV2 gene in *Candida albicans* causes a pronounced starvation-cidal phenotype and significantly attenuates fungal virulence, providing biological validation of AHAS as an antifungal target [2]. Moreover, several AHAS-inhibiting sulfonylurea and triazolopyrimidine herbicides inhibit *C. albicans* AHAS at nanomolar or subnanomolar concentrations and exhibit antifun-

Check for updates

Academic Editor: Julio A. Seijas

Published: 3 November 2026

**Copyright:** © 2026 by the authors. Licensee MDPI, Basel, Switzerland. This article is an open access article distributed under the terms and conditions of the Creative Commons Attribution (CC BY) license.

gal activity in cellular and animal models [3]. These findings support the repurposing of AHAS-inhibiting herbicides as starting scaffolds for antifungal drug discovery.

Our previous computational study of AHAS-mediated herbicide resistance in *Ambrosia artemisiifolia* showed that a resistance-associated tryptophan-to-leucine substitution can alter the inhibitor-binding interface by disrupting wild-type interactions and promoting alternative contacts [4]. These findings highlight how target-site substitutions may affect inhibitor recognition and provide a useful framework for investigating potential resistance mechanisms in fungal AHAS.

In this study, an integrated computational approach combining molecular docking, MM/GBSA binding-energy calculations, pharmacophore modeling, enrichment analysis, and atom-based 3D-QSAR was employed to characterize the structural requirements for AHAS inhibition. The main objectives were to identify molecular interactions and pharmacophoric features associated with antifungal activity and to develop validated models suitable for the virtual screening and prioritization of novel AHAS inhibitors.

## 2. Materials and Methods

### *2.1. Molecular Docking Protocol*

For the molecular docking study, the crystal structure of *C. albicans* AHAS in complex with the herbicide metosulam (PDB ID: 6DER) was selected [3]. The dimeric AHAS enzyme was prepared using Schrödinger's Protein Preparation Workflow [5]. Water molecules were removed, whereas the cofactors represented in the crystallographic structure, flavin adenine dinucleotide (FAD), thiamine thiazolone diphosphate (ThThDP), thiamine aminoethenethiol diphosphate (ThAthDP), and $Mg^{2+}$, were retained. Structural inconsistencies were corrected, and the hydrogen-bonding network was optimized. Finally, restrained energy minimization was performed using the default settings to relieve steric clashes and optimize the overall geometry.

Ligands were prepared using LigPrep [6], with relevant protonation states generated over a pH range of 5.5–7.5. The OPLS4 force field was used, and tautomers and stereoisomers were generated where appropriate.

Docking simulations were performed using Glide SP [7] with default parameters and two poses per ligand were retained. The docking grid was centered on metosulam, and no positional constraints were applied.

### *2.2. Molecular Mechanics Generalized Born Surface Area (MM/GBSA)*

The Prime MM/GBSA method [8] was used to estimate relative ligand-binding energies and rescore the selected docking poses. MM/GBSA rescoring can improve docking-based ranking, although its performance is system-dependent and the calculated values should be interpreted as approximate estimates [9]. The docking poses were used as inputs for MM/GBSA computations with the OPLS4 force field and VSGB 2.0 solvation model settings. The binding free energy estimate was calculated as $\Delta G_{bind} = E_{complex} - (E_{protein} + E_{ligand})$ [10], where the energy terms comprise molecular mechanics and solvation contributions [11].

### *2.3. Pharmacophore Modeling Protocol*

Pharmacophore models were generated from docked compounds with experimentally determined inhibitory activities. The Develop Pharmacophore Model tool from Phase Schrödinger [12] was used with the "Create pharmacophore model" and "Multiple ligands" options. The docking poses provided the prealigned ligand conformations. Experimental Ki values were converted to pKi values, defined as −log10(Ki in mol/L). Compounds with pKi ≥ 7 were classified as active, whereas compounds with pKi ≤ 6.5 were classified as

inactive; compounds with intermediate values were not assigned to either class. Hypotheses containing three to five pharmacophore features were generated. Model validation was performed using active–decoy enrichment analysis and atom-based 3D-QSAR.

For enrichment analysis, known active inhibitors were combined with property-matched decoys to assess the ability of each hypothesis to prioritize active compounds. To prevent data leakage, active compounds used to generate the pharmacophore hypotheses were excluded from the validation set. The resulting set comprised 52 known active compounds from the original collection of 76 AHAS inhibitors and 2350 putative decoys generated using the DUD-E platform [13]. The decoys were matched to the ligands using six physicochemical properties: molecular weight, miLogP, number of rotatable bonds, numbers of hydrogen-bond donors and acceptors, and net charge. Ligand protonation states in the pH range 6–8 were generated using Epik, and molecular properties were cal-culated using Molinspiration. Candidate decoys were drawn from the ZINC database us-ing a dynamic property-matching protocol adapted to the local chemical space. ECFP4 fingerprints were used to remove candidates with high structural similarity to the ligands. Duplicate decoys were removed, and the remaining compounds were distributed as evenly as possible among the ligands, with up to 50 decoys randomly selected per ligand [13].

Second, the atom-based 3D-QSAR methodology implemented in Phase was used to assess the predictive performance of the HHNR hypothesis. Compounds aligned to HHNR were divided into a training set (83%) and a test set (17%). Experimental Ki values were converted to pKi values. The 3D-QSAR model was constructed using a grid spacing of 1 Å and two partial least-squares (PLS) factors; the leave-out value was set to one lig-and.

## 3. Results and Discussion

Based on the literature [3,14,15], a set of AHAS inhibitors was compiled, most of which were developed as herbicides. Several of these compounds have also been reported to inhibit C. albicans AHAS.

### *3.1. Molecular Docking*

Metosulam, the most potent compound in the experimental dataset [3], ranked 18th according to the GlideScore but ranked first after MM/GBSA rescoring, with a calculated ΔGbind of −48.10 kcal/mol. For metosulam, MM/GBSA therefore produced a ranking that was more consistent with experimental potency than the initial docking score. However, performance across the complete compound set should be quantified before drawing broader conclusions regarding predictive superiority.

Docking analysis identified hydrogen bonds involving Lys247 and Arg376 and π–π stacking interactions involving Trp582 and Phe197. The interactions involving Lys247, Arg376, and Trp582 are consistent with crystallographic observations [3]. Additional hydrogen bonds with Gly654, Ala112, and Ala113 were predicted for some compounds. Other noncovalent contacts involved Ala196, Phe197, Gln198, Trp582, Val579, Met350, Met578, Phe586, Ala653, Val187, Pro188, Ala191, and Ala113 (Figure 1). Crystallographic studies identify the π-stacking interaction with Trp582 and the carbon–π interaction with Pro188 as important anchoring contacts [3]. In the analyzed docking poses, Arg376 and Lys247 formed the largest numbers of hydrogen bonds with the ligands.

No direct ligand–cofactor contacts were identified in the analyzed docking poses. FAD formed a π–π stacking interaction with Phe197, which may act as a bridge between the cofactor and some ligands (Figure 1).

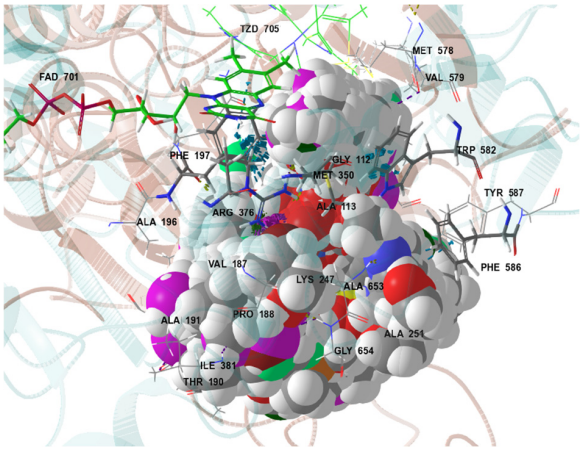
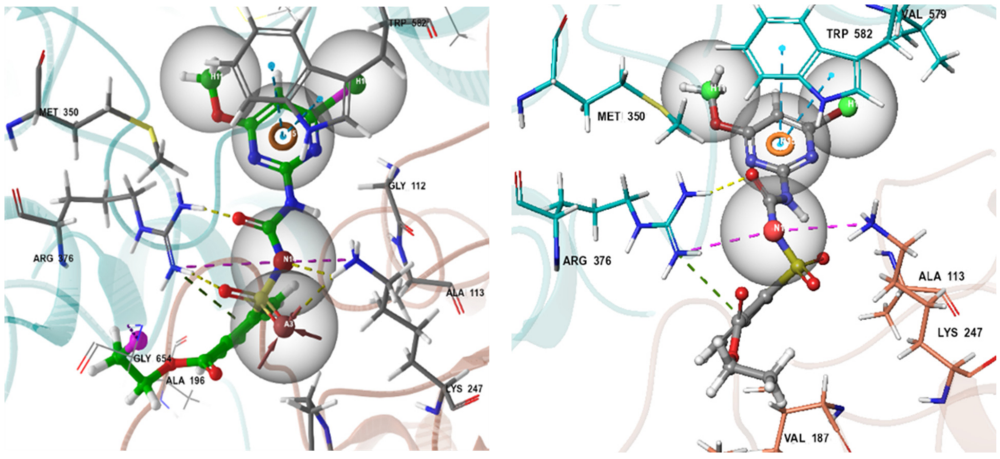



**Figure 1.** Herbicides in the binding site of *C. albicans* AHAS. Cofactors are shown in green. Ligand–residue interactions are colored as follows: magenta, salt bridges; blue, π–π stacking interactions; purple, halogen bonds.

### *3.2. Pharmacophore Modeling*

To identify common structural features associated with AHAS inhibition, pharmacophore hypotheses were generated from 41 compounds with experimentally determined activities and docking-derived alignments. The compounds were classified as active or inactive according to their pKi values. Thirty hypotheses containing three to five features were generated. The feature types were a hydrogen-bond acceptor (A), hydrophobic center (H), negative ionic center (N), and aromatic ring (R). The AHHNR hypothesis (Figure 2a) had the highest survival score (5.663) and was selected for further analysis. The HHNR hypothesis was also selected because 24 active compounds matched the model and its features mapped to interactions in the AHAS binding site. HHNR (Figure 2b) contains two hydrophobic centers, one negative ionic center, and one aromatic-ring feature. In the mapped poses, aromatic groups matching the R feature formed π–π stacking interactions with Trp582, whereas groups matching the N feature formed ionic interactions with Arg376 and Lys247. The hydrophobic features occupied regions surrounded by nonpolar residues. The HHNR hypothesis had a survival score of 5.081. Interfeature distances are reported in Table S1 (slide presentation).




(**a**) (**b**)

**Figure 2.** AHHNR (**a**) and HHNR (**b**) pharmacophore hypotheses mapped onto the reference ligands CHEMBL2313156 (**a**) and CHEMBL2312866 (**b**) in the binding site of *C. albicans* AHAS. The hypotheses contain hydrophobic centers (H), aromatic-ring features (R), and negative ionic centers (N); AHHNR additionally contains a hydrogen-bond acceptor (A).

3.2.1. Enrichment Analysis

The AHHNR and HHNR hypotheses were evaluated using the active and decoy sets; the results are presented in Table 1.

**Table 1.** Comparative enrichment analysis of the AHHNR and HHNR pharmacophore hypotheses.

| Parameter | AHHNR | HHNR | Interpretation |
|---|---|---|---|
| ROC AUC | 0.69 | 0.77 | HHNR better |
| BEDROC ($\alpha = 8$) | 0.607 | 0.779 | HHNR better |
| RIE | 8.27 | 12.87 | HHNR better |
| Area under accumulation curve | 0.81 | 0.87 | HHNR better |
| Retrieved actives | 37/52 | 40/52 | HHNR better |
| Top 1% decoys—active [a] | 23.10% | 76.90% | HHNR much better |
| Top 2% decoys—active [a] | 36.50% | 76.90% | HHNR much better |
| Top 5% decoys—active [a] | 57.70% | 76.90% | HHNR better |
| Top 10% decoys—active [a] | 71.20% | 76.90% | HHNR slightly better |
| Top 1% results—active [b] | 17.30% | 42.30% | HHNR better |
| Top 2% results—active[b] | 32.70% | 73.10% | HHNR much better |
| Top 5% results—active [b] | 53.80% | 76.90% | HHNR better |
| Top 10% results—active [b] | 71.20% | 76.90% | HHNR slightly better |
| EF at 1% sample size | 17× | 44× | HHNR much better |
| EF at 2% sample size | 16× | 36× | HHNR much better |
| EF at 5% sample size | 11× | 15× | HHNR better |
| EF at 10% sample size | 7.1× | 7.7× | HHNR slightly better |
| Hit rate top 50 | 34% | 76% | HHNR much better |
| Hit rate top 100 | 23% | 40% | HHNR better |
| Hit rate top 200 | 17.50% | 20% | HHNR better |
| Hit rate top 300 | 12.30% | 13.30% | HHNR slightly better |

[a] Percentage of actives in top N% of decoy results; [b] percentage of actives in top N% of results; Boltzmann-enhanced discrimination of receiver operating characteristic; EF, enrichment factor; RIE, robust initial enhancement; ROC AUC, area under the receiver operating characteristic curve.

The enrichment analysis revealed a clear difference in the screening performance of the two pharmacophore hypotheses. While both approaches demonstrated the ability to prioritize active compounds, the second hypothesis showed substantially superior performance. Its ROC AUC increased from 0.69 to 0.77, indicating improved overall discrimination between active compounds and decoys, while the BEDROC value increased from 0.607 to 0.779 ($\alpha = 8$), highlighting a considerably stronger early recognition of active compounds. This improvement was also reflected in the RIE and accumulation curve values, which increased from 8.27 to 12.87 and from 0.81 to 0.87, respectively.

The difference was particularly pronounced in the early stages of the ranking. Within the top 1% of the ranked results, the second hypothesis (HHNR) recovered 42.3% of the known actives, compared with 17.30% for the first hypothesis (AHHNR). At the top 2%, the corresponding values were 73.1% and 32.7%, respectively. The enrichment factors at the top 1% were 44-fold for the second hypothesis and 17-fold for the first hypothesis. Overall, these findings indicate that the HHNR pharmacophore hypothesis provides a more effective model for early-stage virtual screening and hit prioritization, with greater potential to reduce the number of compounds requiring subsequent experimental validation.

3.2.2. Atom-Based 3D-QSAR Analysis

An atom-based 3D-QSAR model was generated from the alignment of inhibitors to the HHNR hypothesis. A total of 24 active, docked compounds were aligned to HHNR. The training/test-set allocation and the experimental and predicted activities are provided in Table S3 (slide presentation). The statistical parameters of the best QSAR model developed using 2 PLS factors for the HHNR hypothesis are discussed below.

The model showed a strong training-set fit ($R^2 = 0.909$, SD = 0.197, F = 84.9, $p = 1.43 \times 10^{-9}$) and a high Pearson correlation for the test-set predictions (r = 0.901), with an RMSE of 0.37. However, $Q^2 = 0.538$ indicates only moderate predictive performance and limited robustness. Figure 3 presents the relationship between predicted and observed activity in the training and test datasets. Each point represents an individual observation, with predicted activity plotted on the x-axis and observed activity on the y-axis. The dotted lines represent the fitted linear regression lines. Both datasets exhibit a positive linear association between predicted and observed activity, suggesting good predictive performance, particularly in the training set. The test set shows the same overall trend, although the smaller number of observations results in greater uncertainty in the relationship.

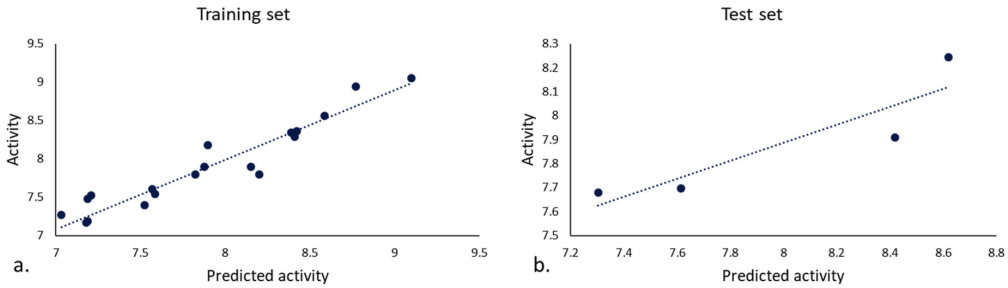



**Figure 3.** Scatter plots of experimental versus predicted activity (pKi) for the training set (**a**) and the test set (**b**).

The model should therefore be regarded as exploratory rather than fully validated. The docking results provide structural context for the observed structure–activity relationships, but prospective testing on an in-dependent compound set is required. These limitations likely reflect, at least in part, the restricted dataset and the small test set.

## 4. Conclusions

The present study provides a structure-based framework for identifying potential *C. albicans* AHAS inhibitors. Molecular docking identified binding-site interactions consistent with key crystallographic contacts, and MM/GBSA rescoring ranked metosulam as the compound with the most favorable calculated binding energy. Among the evaluated pharmacophore hypotheses, HHNR showed the strongest enrichment and early-recognition performance. The HHNR-based atom-based 3D-QSAR model provided a strong training-set fit but only moderate predictive performance, owing in part to the limited dataset. HHNR may therefore serve as an exploratory filter for prioritizing compounds for prospective testing. Experimental studies are required to confirm AHAS inhibition, antifungal efficacy, selectivity, resistance liability, and safety.

**Supplementary Materials:** The following supporting information can be downloaded at: https://www.mdpi.com/article/10.3390/chemproc2026022122/s1, Slide Presentation; Figure S1: Herbicides in the binding site of C. albicans AHAS. Cofactors are shown in green. Ligand–residue interactions are colored as follows: magenta, salt bridges; blue, π–π stacking inter-actions; purple, halogen bonds; Figure S2: AHHNR (a) and HHNR (b) pharmacophore hypotheses mapped onto the reference ligands CHEMBL2313156 (a) and CHEMBL2312866 (b), in the binding site of C. albicans AHAS. The hypotheses contain hydrophobic centers (H), aromatic-ring features (R), and negative ionic centers (N); AHHNR additionally contains a hydrogen-bond acceptor (A); Figure S3: Scatter plots of experimental versus predicted activity (pKi) for the training set (a) and the test set (b); Table S1: Distances between pharmacophore centers in Angstroms for (a) AHHNR and (b) HHNR pharmacophore models; Table S2: Comparative enrichment analysis of the AHHNR and HHNR pharmacophore hypotheses; Table S3: QSAR model datasets and comparison of experimental and predicted activities.

**Author Contributions:** Conceptualization, A.B.; methodology, A.B., R.D.S. and S.A.M.; validation, A.B. and R.D.S.; writing—original draft preparation, A.B. and R.D.S.; writing—review and editing, A.B., R.D.S. and S.A.M.; supervision, A.B.; All authors have read and agreed to the published version of the manuscript.

**Funding:** This research received no external funding.

**Institutional Review Board Statement:** Not applicable.

**Informed Consent Statement:** Not applicable.

**Data Availability Statement:** The data presented in this study are available on request from the corresponding author.

**Acknowledgments:** This study was supported by Project 1.1 of the "Coriolan Dragulescu" Institute of Chemistry of the Romanian Academy. During the preparation of this manuscript/study, the author(s) used OpenAI's ChatGPT (GPT-5.6 Luna) for language editing and to improve the clarity, coherence, and logical organization of the ideas presented. AI tools were also used to format the references. The authors have reviewed and edited the output and take full responsibility for the content of this publication.

**Conflicts of Interest:** The authors declare no conflicts of interest.

## References

1. McCourt, J.A.; Duggleby, R.G. Acetohydroxyacid synthase and its role in the biosynthetic pathway for branched-chain amino acids. *Amino Acids* **2006**, *31*, 173–210. [CrossRef] [PubMed]
2. Kingsbury, J.M.; McCusker, J.H. Cytocidal amino acid starvation of Saccharomyces cerevisiae and Candida albicans aceto-lactate synthase (ilv2Δ) mutants is influenced by the carbon source and rapamycin. *Microbiology* **2010**, *156*, 929–939. [CrossRef] [PubMed]
3. Garcia, M.D.; Chua, S.M.H.; Low, Y.-S.; Lee, Y.-T.; Agnew-Francis, K.; Wang, J.-G.; Nouwens, A.; Lonhienne, T.; Williams, C.M.; Fraser, J.A.; et al. Commercial AHAS-inhibiting herbicides are promising drug leads for the treatment of human fungal pathogenic infections. *Proc. Natl. Acad. Sci. USA* **2018**, *115*, E9649–E9658. [CrossRef] [PubMed]
4. Borota, A.; Funar-Timofei, S.; Neanu, C.; Halip, L.; Savulescu, R. Computational insights into herbicide resistance via acetohydroxyacid synthase in *Ambrosia artemisiifolia*. *Comput. Biol. Chem.* **2026**, *123*, 108959. [CrossRef] [PubMed]
5. Schrödinger, LLC. *Schrödinger Release 2025-2: Protein Preparation Wizard*; Epik; Impact; Prime; Schrödinger, LLC: New York, NY, USA, 2025.
6. Schrödinger, LLC. *Schrödinger Release 2025-2: LigPrep*; Schrödinger, LLC: New York, NY, USA, 2025.
7. Schrödinger, LLC. *Schrödinger Release 2025-2: Glide*; Schrödinger, LLC: New York, NY, USA, 2025.
8. Schrödinger, LLC. *Schrödinger Release 2025-2: Prime*; Schrödinger, LLC: New York, NY, USA, 2025.
9. Wang, E.; Sun, H.; Wang, J.; Wang, Z.; Liu, H.; Zhang, J.Z.H.; Hou, T. End-point binding free energy calculation with MM/PBSA and MM/GBSA: Strategies and applications in drug design. *Chem. Rev.* **2019**, *119*, 9478–9508. [CrossRef] [PubMed]
10. Genheden, S.; Ryde, U. The MM/PBSA and MM/GBSA methods to estimate ligand-binding affinities. *Expert Opin. Drug Discov.* **2015**, *10*, 449–461. [CrossRef] [PubMed]
11. Li, J.; Abel, R.; Zhu, K.; Cao, Y.; Zhao, S.; Friesner, R.A. The VSGB 2.0 model: A next-generation energy model for high-resolution protein structure modeling. *Proteins* **2011**, *79*, 2794–2812. [CrossRef] [PubMed]
12. Schrödinger, LLC. *Schrödinger Release 2025-2: Phase*; Schrödinger, LLC: New York, NY, USA, 2025.
13. Mysinger, M.M.; Carchia, M.; Irwin, J.J.; Shoichet, B.K. Directory of useful decoys, enhanced (DUD-E): Better ligands and decoys for better benchmarking. *J. Med. Chem.* **2012**, *55*, 6582–6594. [CrossRef] [PubMed]
14. Lonhienne, T.; Garcia, M.D.; Low, Y.-S.; Guddat, L.W. Herbicides that inhibit acetolactate synthase. *Front. Agric. Sci. Eng.* **2022**, *9*, 155–160. [CrossRef]
15. Lee, Y.-T.; Cui, C.-J.; Chow, E.W.L.; Pue, N.; Lonhienne, T.; Wang, J.-G.; Fraser, J.A.; Guddat, L.W. Sulfonylureas have antifungal activity and are potent inhibitors of Candida albicans acetohydroxyacid synthase. *J. Med. Chem.* **2013**, *56*, 210–219. [CrossRef] [PubMed]

**Disclaimer/Publisher's Note:** The statements, opinions and data contained in all publications are solely those of the individual author(s) and contributor(s) and not of MDPI and/or the editor(s). MDPI and/or the editor(s) disclaim responsibility for any injury to people or property resulting from any ideas, methods, instructions or products referred to in the content.